





Results from a new flowing liquid Li limiter with TZM substrate during high confinement plasmas in the EAST device

Cite as: Phys. Plasmas **27**, 052506 (2020); <https://doi.org/10.1063/1.5143179>

Submitted: 22 December 2019 . Accepted: 16 April 2020 . Published Online: 12 May 2020

G. Z. Zuo, C. L. Li, R. Maingi, X. C. Meng, Z. Sun, W. Xu, Y. Z. Qian, M. Huang, Z. L. Tang, D. H. Zhang, L. Zhang , Y. J. Chen, S. T. Mao, Y. M. Wang , H. L. Zhao, D. Andruczyk , K. Tritz, X. Z. Gong, J. S. Hu , and EAST Team



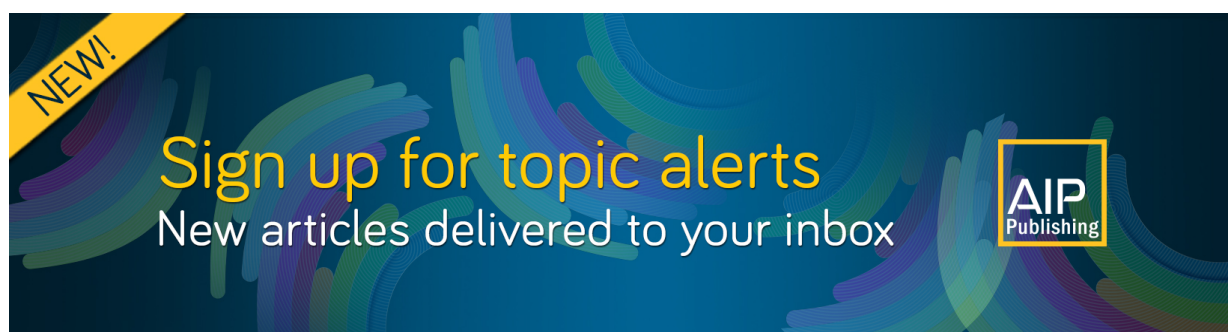
View Online



Export Citation



CrossMark



Results from a new flowing liquid Li limiter with TZM substrate during high confinement plasmas in the EAST device

Cite as: Phys. Plasmas **27**, 052506 (2020); doi: 10.1063/1.5143179

Submitted: 22 December 2019 · Accepted: 16 April 2020 ·

Published Online: 12 May 2020







View Online



Export Citation



CrossMark

G. Z. Zuo,^{1,a),b)} C. L. Li,^{1,2} R. Maingi,³ X. C. Meng,^{1,4} Z. Sun,^{1,3} W. Xu,^{1,4} Y. Z. Qian,^{1,2} M. Huang,¹ Z. L. Tang,¹ D. H. Zhang,¹ L. Zhang,¹  Y. J. Chen,¹ S. T. Mao,¹ Y. M. Wang,¹  H. L. Zhao,¹ D. Andruczyk,⁵  K. Tritz,⁶ X. Z. Gong,¹ J. S. Hu,^{1,7,b)} 
and EAST Team^{c)}

AFFILIATIONS

¹Institute of Plasma Physics, Chinese Academy of Sciences, Hefei, Anhui 230031, China

²University of Science and Technology of China, Hefei, Anhui 230026, China

³Plasma Physics Laboratory, Princeton University, Princeton, New Jersey 08543, USA

⁴Advanced Energy Research Center, Shenzhen University, Shenzhen 518060, China

⁵Center for Plasma Material Interactions, University of Illinois, Urbana-Champaign, Maryland 21211, USA

⁶Johns Hopkins University, Baltimore, Maryland 21211, USA

⁷CAS Key Laboratory of Photovoltaic and Energy Conservation Materials, Hefei 230031, China

Note: This paper is part of the Special Collection: Papers from the 61st Annual Meeting of the APS Division of Plasma Physics.

Note: Paper Y13 2, Bull. Am. Phys. Soc. **64** (2019).

^{a)}Invited speaker.

^{b)}Authors to whom correspondence should be addressed: zuoguizh@ipp.ac.cn and hujs@ipp.ac.cn

^{c)}See Appendix of B. N. Wan et al., Nucl. Fusion **59**, 112003 (2019).

ABSTRACT

A third generation flowing liquid lithium (FLiLi) limiter with a substrate made of TZM, an alloy with >99% Mo, was fabricated by conventional manufacturing techniques. TZM has a high corrosion resistance, a high sputtering threshold, and a good wettability to Li, as compared to stainless steel (SS), which had been used as an FLiLi substrate surface in 2014 and 2016. The third generation FLiLi was inserted into the edge in EAST H-mode plasmas in an upper single-null configuration with an ion grad-B drift toward the upper divertor with a limiter temperature of 330–380 °C and an auxiliary heating power of about 2–8 MW. Analysis has shown that by using TZM FLiLi, fuel particle recycling continuously decreased and near-complete edge localized mode elimination was achieved in H-mode plasmas with RF-only heating. The main impurities during the initial FLiLi discharges were Mo, Fe, and W resulting from strong plasma interaction at the Mo plate side, the SS collector, and the upper W divertor. Plasma stored energy increased by about 10 kJ in subsequent FLiLi discharges due to decreased impurity radiation. Engineering analysis shows a uniform lithium flow with an ~80% Li coverage ratio on the limiter surface, similar to the second FLiLi, even though only one of two J × B pumps was functioning. Despite technical difficulties, the FLiLi gen.3 improved the overall plasma performance, providing support for flowing liquid Li plasma facing component applications in present and future devices.

Published under license by AIP Publishing. <https://doi.org/10.1063/1.5143179>

I. INTRODUCTION

Traditional solid plasma facing materials (PFMs) face severe challenges from extreme particle and heat flux in future devices.¹ They not only produce impurity and fuel particle recycling, which result in deteriorated energy confinement and uncontrollable plasma density, but also cause wall material erosion and damage. In contrast, liquid

metals, especially liquid lithium (Li), are promising with regard to the handling of particle and heat flux, and can self-heal to prevent wall erosion. Therefore, liquid metals are being studied as an alternative PFM for future devices.^{2,3}

Li is an excellent PFM material to improve plasma performance due to its physical and chemical properties.^{4–6} Li is a low $Z = 3$ metal,

TABLE I. Comparison of key physical parameters between SS and TZM.

	SS	TZM
Thermal conductivity (λ) (W/m K)	16–21 (100–500 °C)	126
Melting point (K)	1398–1454 (304 SS)	2617
Sputtering yield with 100 eV D ⁺ (atom/ion)	~0.045 (Fe)	~0.0123 (Mo)
Corrosivity in liquid Li with 330 °C ($\mu\text{m/a}$)	~0.58	~0.34
Liquid Li critical wettability temperature (°C)	256	336

which can be compatible with high temperature core plasmas as long as the Li concentration is <20%. Furthermore, Li has a low melting point at 180 °C, which helps Li to easily liquify. For particle pumping, the liquid Li operating temperature is about 200–400 °C. To realize Li vapor shielding,^{7–9} the Li operational temperature is about 500–800 °C. Finally, Li can capture D, T, O, and other impurities due to its strong chemical activity to achieve a strong divertor particle pumping (e.g., low-recycling). Therefore, Li has been used in tokamaks through Li coating,^{10–13} Li injection,^{14–16} and liquid Li walls^{17–22} to improve plasma confinement by reducing recycling and impurities, reducing the L–H power threshold,^{23,24} mitigating the edge localized modes (ELMs), and improving the heat removal capacity.

To explore the use as a PFM, liquid Li limiter or divertor experiments have been performed in several devices, such as FTU,^{25–27} T-11M,⁹ and NSTX.^{7,28} Different types of liquid Li walls were designed and tested, including free surface, capillary porous surface, and trench structural designs. Besides the achievement of lower recycling^{7,22,27} and impurity levels with a correspondingly higher plasma performance, the liquid Li experiments also confirmed that the wall heat load was mitigated due to an increased Li efflux and enhanced edge radiation from the liquid Li limiter or divertor surfaces. In Institute of Plasma Physics Chinese Academy of Sciences, liquid Li wall experiments were first investigated in HT-7,^{29,30} and an initial flowing liquid Li design was also tested.³¹ It was found that Li droplets were injected into the plasma due to the $\mathbf{J} \times \mathbf{B}$ force, which lead to a plasma disruption. Furthermore, a thin film Li or a capillary porous system (CPS) could reduce this Li ejection.³² Finally, Li wetting was important for the uniform Li coverage on the Li limiter surface.

Based on the liquid Li experiments in HT-7, we developed a slowly flowing thin Li film for EAST.³³ By using thin Li film, Li droplet ejection should be reduced by relying on the liquid Li surface tension to counteract the $\mathbf{J} \times \mathbf{B}$ force. The Li flow rate was designed for $\sim 2 \text{ cm}^3 \text{ s}^{-1}$ to effectively pump particles from the plasma. For heat flux control, the design still used traditional heat sink and cooling pipes to remove the heat flux, and heat removal directly by liquid Li convection is ignored.

Two generations of flowing liquid Li limiters have been developed in EAST.^{17,20} The limiter was composed of a distributor, a guide plate, a collector, and an electro-magnetic (EM) pump. The guide plate included a stainless steel (SS) surface layer and a copper (Cu) heat sink. Both the electrical heating cartridge and the cooling pipe were inserted into the limiter heat sink to provide the heating and cooling of the flowing liquid lithium (FLiLi) system during the plasma discharge. While using the first and second generation FLiLis, it was noted that the liquid Li flow could be sufficiently driven by the DC EM pump, and, furthermore, the thin Li surface film did indeed reduce the Li droplet ejection. Additionally, improved particle and heat flux control using the flowing

liquid Li and the Li efflux from FLiLi during FLiLi operation were observed. It was also observed that FLiLi was compatible with EAST H-mode operations with a heating power of up to 4.5 MW, i.e., observed concurrent plasma confinement improvement and stable FLiLi operations. Though significant progress has been made in the development of FLiLi and the investigation of the interaction between FLiLi and plasma, the compatibility with higher power operations, such as 5–10 MW, needs further study. Furthermore, the main engineering issues, including the improvement of Li wettability and surface erosion resistance, still need to be resolved. Therefore, a new TZM substrate FLiLi was developed and tested in EAST in 2018.

In this paper, the design of the new TZM substrate FLiLi and key diagnostics are described in Sec. II for the third generation FLiLi system. The main experimental results are presented in Sec. III. Finally, a summary is provided in Sec. IV.

II. EXPERIMENTAL SETUP

A. Design of third generation FLiLi using TZM substrate

TZM (an alloy with >99% Mo) has improved physical properties compared to SS for use as an FLiLi substrate in a fusion environment. TZM has a higher thermal conductivity, a higher melting point, and an increased sputtering threshold compared to SS, as shown in Table I. In the previous two generations of FLiLis, a thin SS layer was used as a limiter substrate material, which needed an additional Cu heat sink to increase the heat removal capacity due to the low thermal conductivity of SS. However, the use of a Cu heat sink has a safety risk due to the high susceptibility of corrosion when Cu contacts liquid Li. Conversely, TZM has good compatibility with liquid Li. Overall, Mo has a superior Li corrosion resistance compared to SS, which has been experimentally confirmed by immersing the Mo and SS sample materials into liquid Li and observing the mass loss. Furthermore, the Li critical wetting temperature on a Mo surface is ~ 80 °C lower than that of an SS surface. Given these considerations, we decided to use TZM as an FLiLi substrate material in the third generation FLiLi. Figure 1 shows two kinds of FLiLi guide plates: Fig. 1(a) shows a combination guide plate with an SS surface layer and a Cu heat sink used in the first and second generation FLiLis, and Fig. 1(b) shows the TZM guide plate in the third generation FLiLi.

The third generation FLiLi system still uses the same auxiliary systems of the previous second generation system, including the EM propulsion system, the Li injector, and the control and measurement system. The FLiLi module is composed of a uniform liquid Li distributor with 200 channels, a TZM guide plate, two liquid Li feed pipes, a cooling pipe, a Li collector, and two DC electro-magnetic (EM) pumps, as shown in Fig. 2. The guide plate has dimensions of 320 mm \times 300 mm. The basic process of the liquid Li operation is that two EM pumps drive the liquid Li flow from

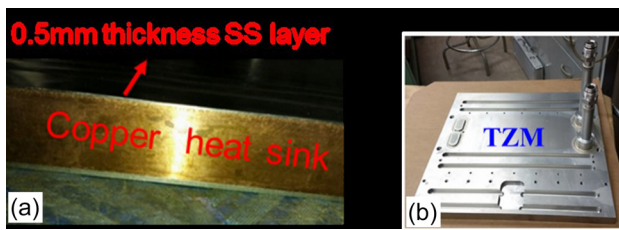


FIG. 1. Two versions of FLiLi guide plates used in FLiLi experiments, (a) a composite guide plate with an SS layer and a Cu heat sink and (b) a TZM substrate guide plate used in the third generation FLiLi.

the bottom collector to the top distributor through the two feed pipes. Li then flows out of the distributor channels down the surface of the front guide plate into the collector. While on the guide plate front surface, the interaction of the flowing liquid Li with the plasma edge serves to remove both fueling particles and impurity fluxes from the plasma.

After final preparations, including pumping, leak detection, and Li injection, FLiLi was inserted into diverted plasmas with a separatrix nominally at $R \sim 2.28\text{--}2.30$ at the vertical location of FLiLi. A range of FLiLi operational conditions, including scans of both limiter position and heating power, were performed in H-mode plasmas with $I_p = 0.45/0.55$ MA, $n_e = 3\text{--}4 \times 10^{19} \text{ m}^{-3}$, and in an upper single-null configuration (USN) with an ITER-like tungsten (W) divertor. The FLiLi position was moved across a range from 0 to 4 cm inside the fixed Mo limiter in EAST. The FLiLi temperature operated in a range of $330\text{--}380^\circ\text{C}$ in discharges with an auxiliary heating power from ~ 2 to 8 MW using lower hybrid wave (LHW) heating systems, electron cyclotron resonance heating (ECRH), and neutral beam injection (NBI). The primary results will be presented in Sec. III.

B. Key diagnostics

A variety of high-performance diagnostics have been developed and used to measure the key plasma parameters in EAST.

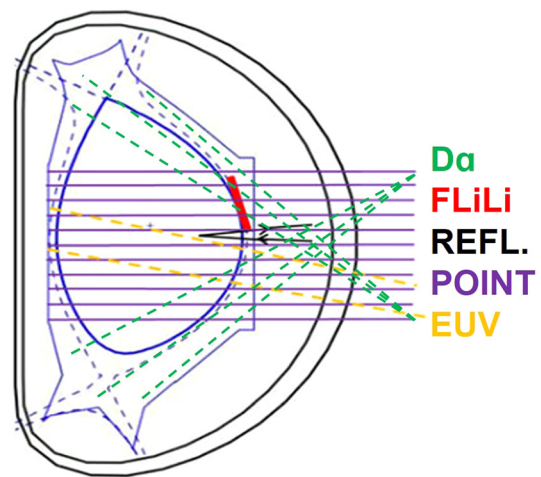


FIG. 3. Schematic drawing of FLiLi installed on the EAST and several key diagnostics. The plasma is operated in an upper single-null divertor configuration. The vertical position for the POINT edge channel is $Z = 42.5$ cm, and the distance is 8.5 cm between two adjacent channels; the vertical position for the REFL is $Z = 3$ cm; the viewing area of the EUV spectrometer is about 30 cm in the vertical direction and 5 cm in the horizontal direction.

The routine diagnostics associated with this work include visible charge-coupled device (CCD) cameras, filterscopes, electron cyclotron emission (ECE), effective ion charge Z_{eff} ,³⁴ and absolute extreme ultraviolet (AXUV) photodiode arrays.³⁵ A flat-field extreme ultraviolet (EUV) spectrometer working in the $20\text{--}500 \text{ \AA}$ wavelength range with a 5 ms frame rate has been newly developed to measure the heavy metallic impurity line emission.³⁶ A fast sweeping reflectometry (refl.) system was used to measure the edge electron density profiles,³⁷ and an 11-channel polarimeter–interferometer (POINT) with a temporal resolution of 1 ms provided the core and edge electron densities.³⁸ The FLiLi position and location of several key diagnostics are shown in Fig. 3.

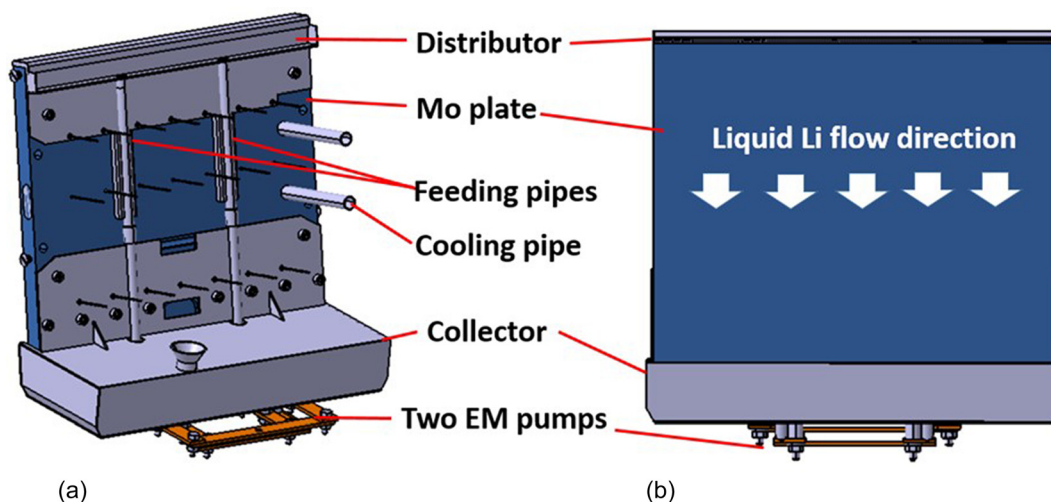


FIG. 2. FLiLi structure drawing, (a) backside photo of FLiLi, and (b) front side photo of FLiLi.

III. RESULTS OF TZM FLiLi EXPOSED TO HIGH CONFINEMENT PLASMAS

A. Gradual reduction of recycling and mitigation of ELMs with FLiLi

During FLiLi operation, it was found that the fuel particle recycling was gradually reduced and ELMs were gradually mitigated. Figure 4 compares three typical shots with similar plasma current, density, heating power, and plasma configuration with $R_{sep.} = 2.29$ m at the FLiLi location. Also shown are the EM driven currents and the different FLiLi positions. Shot 81625, with the limiter positioned at $R = 2.35$ m (FLiLi far away from the plasma), as used as the reference shot and shown in black; shots 81628 and 81632, which have FLiLi closer to the plasma edge with $R = 2.32$ m, are shown as the blue and red traces, respectively. During the first FLiLi shot (81628) and second FLiLi shot (81632), the baseline of Li-II line emission (emitted by Li^+ ions at 548.5 nm) from about 2.5 to 5 s was 1.3 and 1.7 times higher compared to the reference shot (81625). Li line emission enhancement was also observed from about 5 s during shot 81628 and from about 7 s during shot 81632. Figure 5 compares the plasma light emission monitored by a color CCD camera during these plasma discharges at 7.6 s. The green light resulting from Li-II line emission during the first and second FLiLi discharges was strong compared to the little to no green light observed during the reference shot. This indicates that a strong interaction between the FLiLi and the plasma occurs during the FLiLi operation. Additionally, during these discharges, the baseline of D α emission from the lower divertor gradually decreased with an increase in the Li emission from FLiLi, similar to the previous two generations of FLiLi experiments.

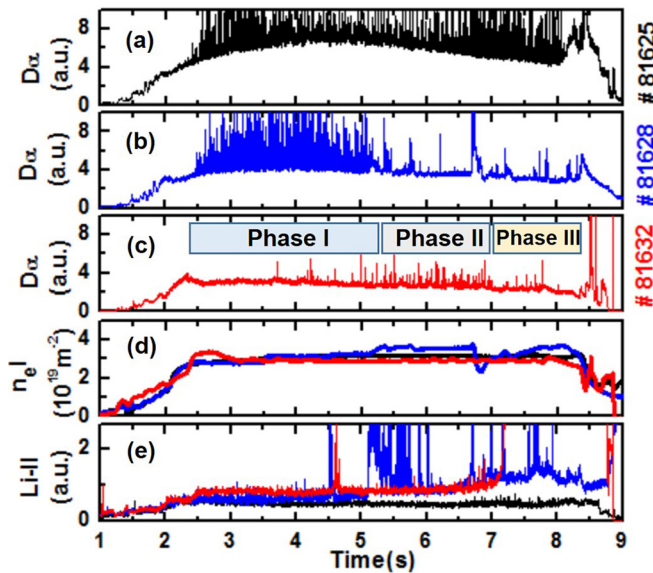


FIG. 4. Comparison of three typical plasmas with and without strong interaction with FLiLi ($I_p = 0.45$ MA; $n_e \sim 3.0 \times 10^{19} \text{ m}^{-2}$, USN, $R_{sep.} = 2.29$ m at the FLiLi position; $P_{heating} \sim 2.5$ MW, $P_{LHW} \sim 2$ MW and $P_{ECRH} \sim 0.5$ MW; shot 81625 with limiter position $R = 2.35$ m, shot 81628 and shot 81632 with limiter position $R = 2.32$ m). Shown are the (a) D α line emission intensity from the lower divertor in shot 81625, (b) D α line emission intensity from the lower divertor in shot 81628, (c) D α line emission intensity from the lower divertor in shot 81632, (d) line-integrated density from POINT, and (e) Li-II line emission intensity in the three shots.

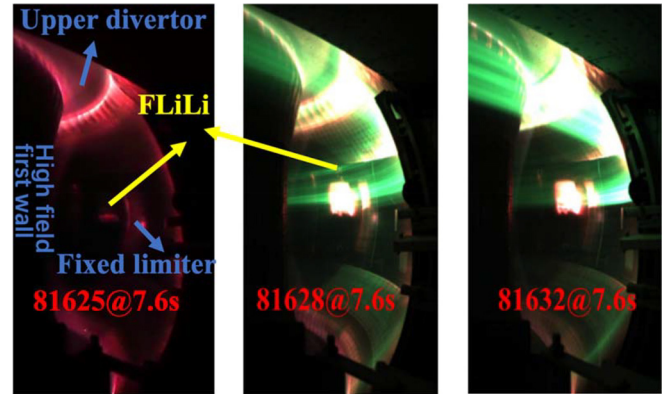


FIG. 5. Comparison of plasma emission with a color camera during three FLiLi shots at 7.6 s.

Furthermore, gradual ELM mitigation during the FLiLi operation was evident from the evolution of D α emission. Compared to the ELM activity in 81625, the first H-mode shot with FLiLi, ELMs appear to be completely suppressed when the Li emission is suddenly enhanced. The second H-mode plasma (shot 81632) can be divided into three phases relative to the different ELM activity. Presumably, this is due to the changes in the wall conditions from the enhanced FLiLi Li efflux, the Li redeposition on the first wall, and the enhanced pumping of fuel particles. It was clearly observed that ELMs were nearly eliminated from 2.5 to about 5.3 s (phase I), with a few low frequency and small ELMs from about 5.3 to 7 s (phase II). Finally, following the enhanced Li emission after 7 s (phase III) during shot 81632, ELMs were again clearly mitigated.

The pedestal density appeared to influence the ELM activity during the FLiLi operation. Figure 6 shows the time evolution of several key parameters in shot 81632. Note that during phase I, the ELM frequency was low. Before about 4.1 s, nearly no ELMs have occurred. Then, from 4.1 s to 5.3 s, the ELM frequency occurred with a frequency of ~ 15 Hz. During this phase, the plasma density measured by edge POINT was low, likely due to the pumping of the fuel particles from the Li film resulting from the FLiLi efflux during shot 81628, which had deposited a thin Li layer on the first wall. During phase II, the ELM frequency gradually increased to near 150 Hz with a concurrent rise in the plasma density, likely due to the gradual degradation of Li film pumping effectiveness. However, after significant Li efflux from FLiLi during this shot, e.g., during phase III, ELM frequency again decreased to a similar level as phase I. Additionally, it was clearly observed that plasma density gradually decreased due to this Li pumping.

Figure 7 compares the edge plasma density from the reflectometry profiles during phase I (3.1 s), phase II (6.0 s), and phase III (7.5 s and 7.7 s) during shot 81632; see also Fig. 6 with FLiLi. The plasma density profile moved outward during phase II, corresponding to an increase in the pedestal density. Shown in Fig. 6(d) is the pedestal electron cyclotron emission, which shows that the electron temperature at the pedestal region remains constant during this shot. Therefore, during phase II, some small, high frequency ELMs were triggered due to this slightly increased pedestal pressure. However, during phase III, due to the Li efflux from FLiLi and redeposition on the surface of the first wall, the pressure profile gradually moved inward with an overall

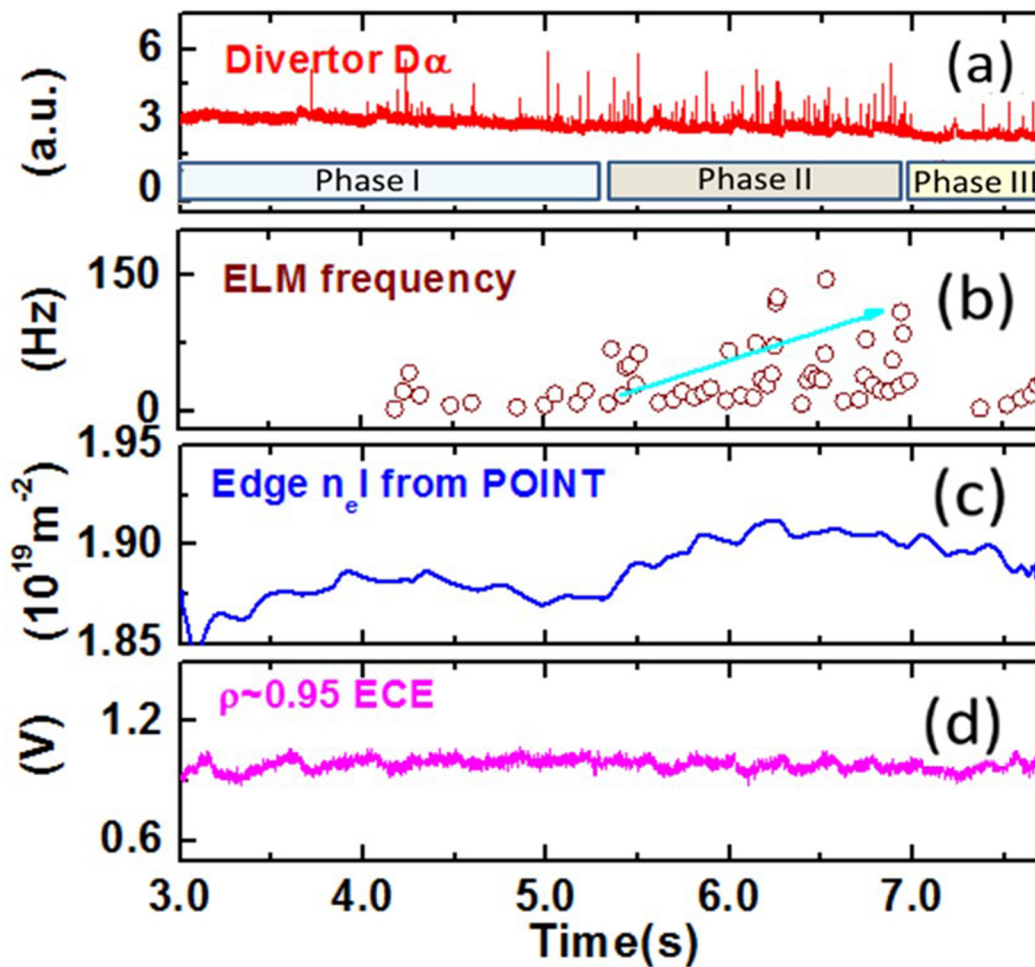


FIG. 6. Time evolution of the main parameters for analyzing the ELM activity change in shot 81632. The data from top to bottom are (a) the $D\alpha$ line emission intensity viewing the lower divertor region; (b) the ELM frequency calculated by $D\alpha$ signal; (c) the edge line-integrated density from POINT; and (d) the pedestal electron cyclotron emission (ECE) signal at $\rho \sim 0.95$; it should be noted that the ECE value can only be used for the qualitative analysis since low hybrid current drive induces superthermal electrons.

reduction in the pedestal pressure and ELM frequency resulting from the gradually increased Li pumping of fuel particles. In conclusion, these ELM mitigated results were obtained through a reduced edge recycling and the modification of the pedestal density and pressure profile in a manner favorable for edge stability, which was similar to the Li wall conditioning results from NSTX and EAST.

Compared to the previous two FLiLi experiments, which observed an ELM-free phase of several tens of ms and to ≥ 200 ms,^{17,39} it was found that the duration of near-complete ELM elimination was expanded up to \sim few seconds. These FLiLi experiments achieved a clear ELM mitigation, which may be beneficial for the control of ELM heat flux in future fusion reactors.

B. Gradual reduction of impurity and improvement of plasma confinement

High-Z impurities strongly influence plasma performance, as observed in the previous FLiLi operations. High impurities mainly

consist of high-Z Fe impurity from the SS substrate sputtering and can accumulate in the plasma core during high heating power and during intermittent ELM-free regimes.¹⁷ Therefore, we need to study the high-Z impurity species evolution during the TZM substrate FLiLi operation. Figure 8 presents a typical EUV spectrum over the wavelength range of 40–200 Å at 3 s and 6 s in EAST shot #81632. It should be noted that there is a strong W-UTA (tungsten unresolved transition array) emission from 45 to 70 Å, which is composed of W^{24+} – W^{45+} .^{40,41} The main high-Z metallic impurities observed in this FLiLi discharge were W, Fe, and Mo.

Based on the above EUV measurement, we investigated the dependence of high-Z impurities, including Mo, W, and Fe, on FLiLi operational parameters. Figure 9 compares the impurity radiation between two typical shots with different FLiLi positions. MoXXIII line emission resulting from the Mo substrate guide plate was three times higher during the FLiLi discharge compared to the reference shot. A further comparison of these two shots shows similar FeXVIII line emission, but W-UTA line emission was slightly higher before 6 s in

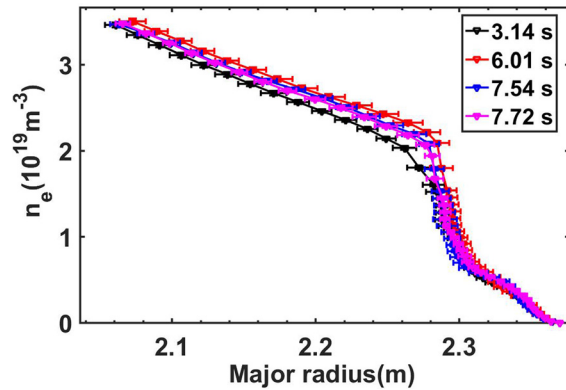


FIG. 7. Comparison of edge electron profiles from the reflectometry during three phases during shot 81632.

the FLiLi discharge. A slightly increased core impurity radiation evaluated by the core XUV signal and the total impurity radiation power was likely due to the sputtering of the Mo guide plate during D plasma bombardment. In addition, it is clearly observed that the high-Z impurity radiation evaluated by MoXXIII, FeXVIII, W-UTA, core XUV, and total impurity radiation remained nearly constant during the FLiLi discharge, except for Mo and Fe impurity bursts resulting from the Mo guide plate and the SS collector sputtering/erosion at about 5 s and 7 s, respectively. However, during the reference shot, the high-Z impurity radiation, especially for W-UTA, demonstrated a gradual accumulation. W impurity accumulation occurred from about 6 s during the reference shot and significantly influenced the core XUV and total impurity radiation.

High-Z impurity radiation measurements gradually decreased with an increasing discharge number during the FLiLi operation. As shown in Fig. 10, high-Z impurity radiation was compared from 4.5 to 7 s during three similar plasma discharges with FLiLi. It was found that Mo, Fe, and W impurities slightly decreased during shot 81633 compared to those of shot 81632. Furthermore, this impurity radiation decreased substantially during shot 81655 compared to those of shots

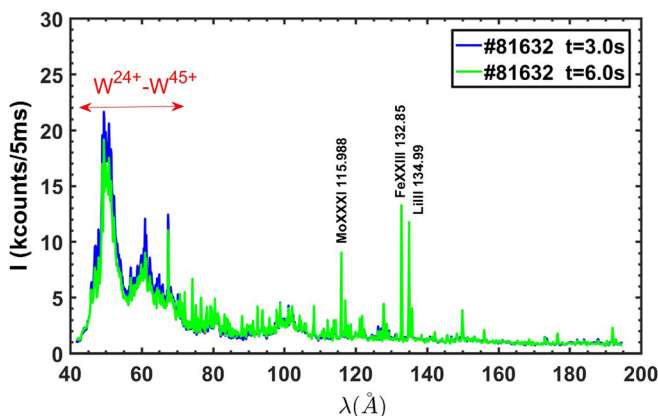


FIG. 8. High-Z impurity radiation information measured by EUV at 3 s and 6 s during shot 81632.

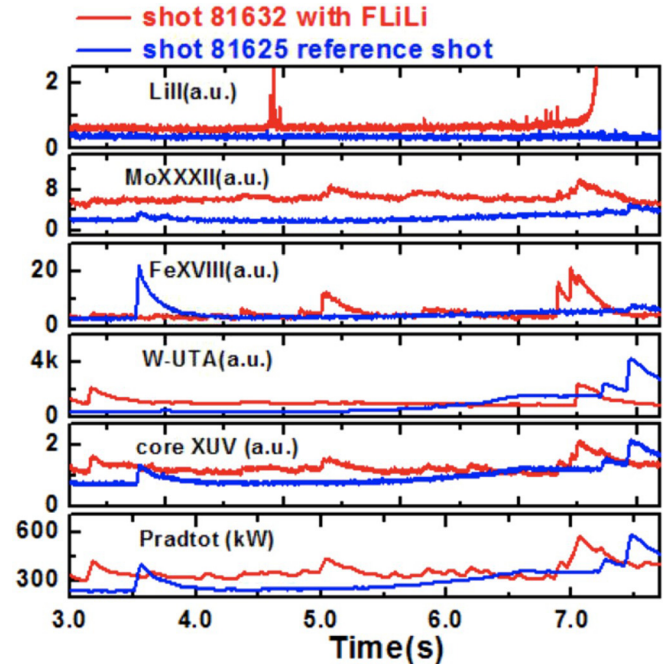


FIG. 9. Comparison of the high-Z impurity level between two typical shots with different FLiLi positions; shown are the Li-II line emission intensity from the lower divertor, the MoXXIII line emission, the FeXVIII line emission, the W-UTA line emission, the core XUV radiation signal, and the total impurity radiation power.

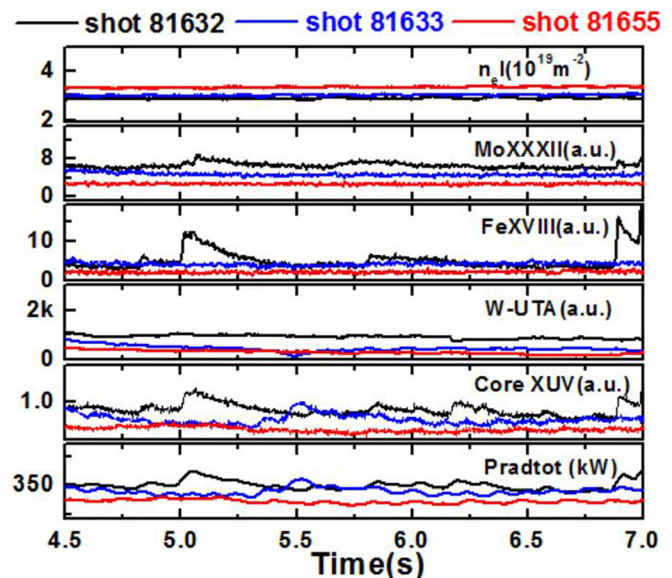


FIG. 10. Comparison of high-Z impurity levels between three typical shots with the FLiLi operation; shown are the line-integrated density from POINT, the MoXXIII line emission, the FeXVIII line emission, the W-UTA line emission, the core XUV radiation signal, and the total impurity radiation power.

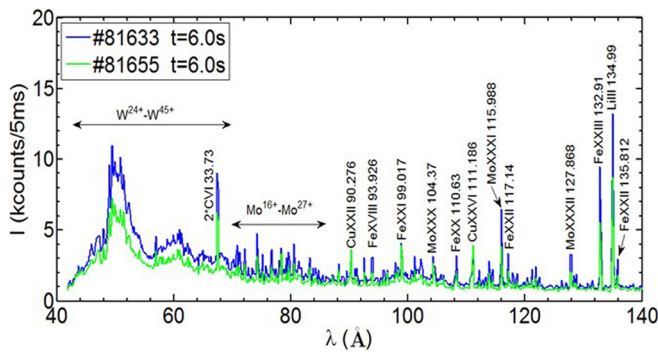


FIG. 11. Comparison of the EUV spectra at 40–140 Å observed with the EUV spectrometer at 6 s in shots 81633 and 81655 ($I_p = 0.45$ MA; $n_{e1} = (3\text{--}3.3) \times 10^{19}$ m $^{-2}$, USN, $R_{sep.} = 2.29$ m at the FLiLi position; $P_{heating} \sim 2.5$ MW, $P_{LHW} \sim 2$ MW, and $P_{ECRH} \sim 0.5$ MW; same limiter position $R = 2.32$ m).

81632 and 81633. Core impurity radiation from XUV measurements and total impurity radiation measurements also gradually decreased. Figure 11 compares the EUV spectra at 40–140 Å observed with the EUV spectrometer at 6 s in shots 81633 and 81655. It was again confirmed that almost all high-Z impurities except Cu decreased after ~ 20 shots of FLiLi operation. It was noted that the DC drive currents of the EM pumps were controlled at 50 and 100 A, respectively, during shot 81633 and shot 81655. This resulted in a larger Li flow rate on the limiter surface during shot 81655 in an attempt to decrease the Mo substrate sputtering.

It should be noted that the low-Z impurity radiation, except Li, also decreased during the FLiLi operation. As shown in Fig. 12, the low-Z impurity radiation was compared during shots 81633 and 81655 with FLiLi. It was also found that CIII, CVI, and OVII

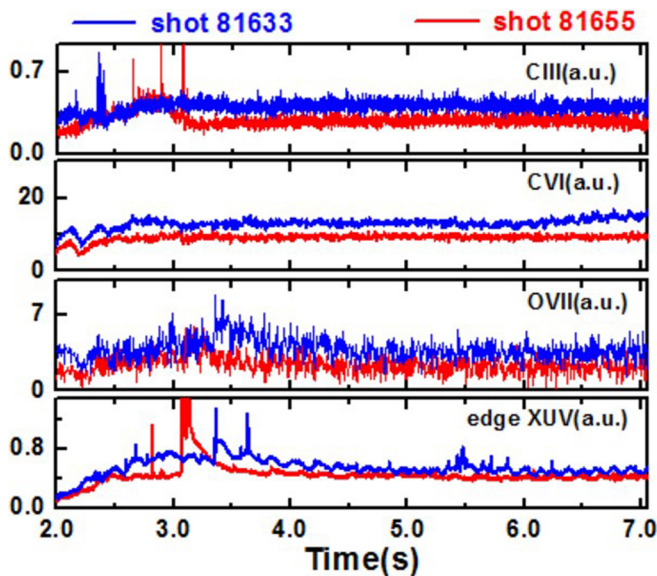


FIG. 12. Comparison of low-Z impurity level between two typical shots with FLiLi; shown are the CIII line emission intensity from the lower divertor, the CVI line emission, the OVII line emission, and the edge XUV radiation signal.

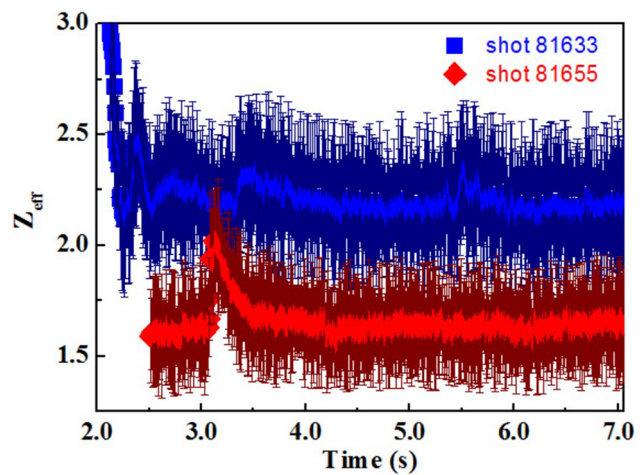


FIG. 13. Comparison of Z_{eff} between two typical shots with FLiLi.

emissions were clearly reduced. Edge impurity radiation measured by the edge XUV diagnostic also decreased, other than the radiation burst resulting from enhanced Li emission due to Li droplet ejection induced by a destructive electromagnetic force at about 3.1 s.

Figure 13 compares the effective ion charge Z_{eff} , which can be used to characterize the global impurity content during shots 81633 and 81655 with the FLiLi operation. It was found that the impurity radiation decreased due to a reduction in Z_{eff} from 2.1 to 1.6. This decreased Z_{eff} resulted from the reduced sputtering of the limiter substrate materials due to a larger Li flow rate on the limiter surface. In addition, with the increase in the Li accumulation from FLiLi due to Li evaporation, sputtering, and Li ejection, more Li was coated on the first wall resulting in the decreased sputtering of the wall materials. We estimated about 2 g Li efflux, i.e., the sum of Li sputtering during discharges and Li evaporation between discharges, entered the plasma, and was then deposited on the first wall over the course of ~ 20 shots.¹⁷ Because of the decreased impurity radiation, the plasma stored energy increased significantly. As shown in Fig. 14, it was found that

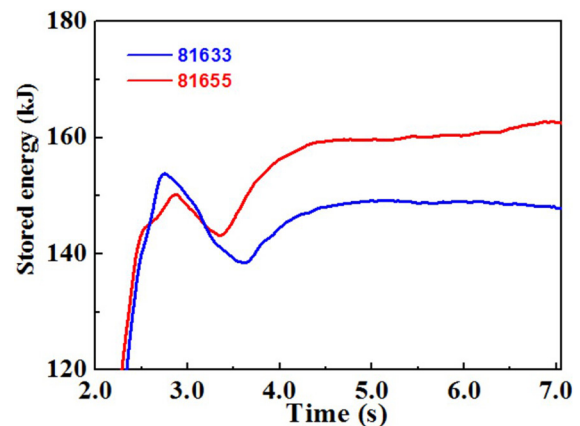


FIG. 14. Comparison of the plasma stored energy between two typical shots with FLiLi.

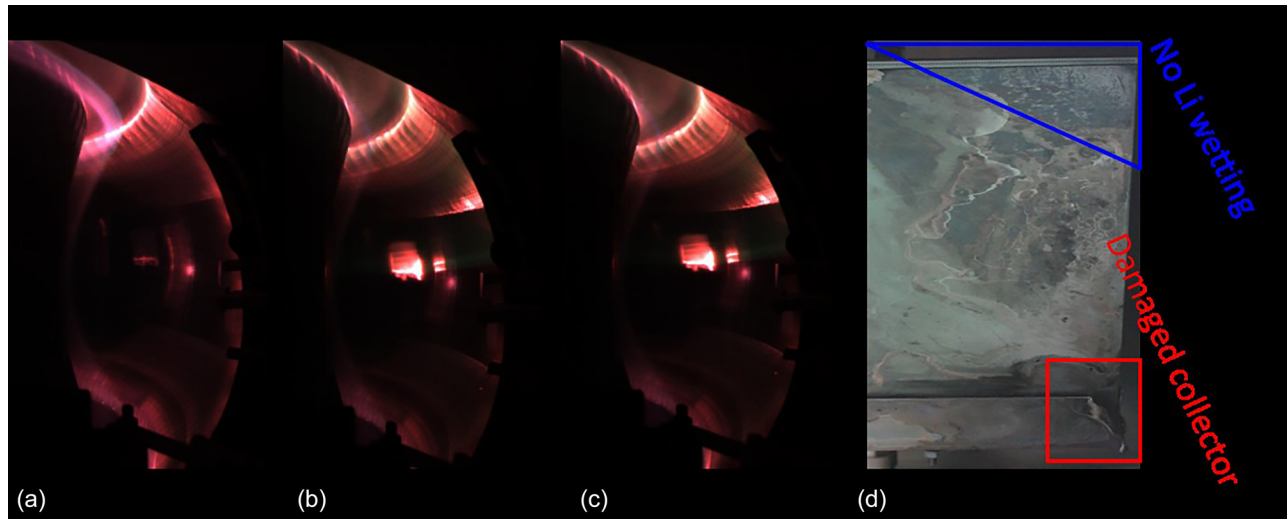


FIG. 15. Comparison of the plasma emission at 5 s using a color camera during three FLiLi shots and FLiLi photo after exposing to air. Shown are the (a) plasma emission in shot 81625, (b) plasma emission in shot 81628, (c) plasma emission in shot 81632, and (d) FLiLi status after the experiment.

the plasma stored energy increased by about 10 kJ in shot 81655 compared to that in shot 81633. It should also be noted that the stored energy decrease between 3 s and 4 s was the result of a W and Cu burst due to a strong interaction between the plasma and the divertor. An increased plasma stored energy was also observed in the Ohmic plasmas during the operation of the previous two generation FLiLis.^{17,20}

C. Flowing liquid Li surface status and related engineering issues

During the FLiLi operation, some engineering issues were observed. Figure 15 compares the plasma emission at 5 s using a color camera during three FLiLi discharges. It can be observed that strong interactions between the plasma and FLiLi occurred at the bottom right of the FLiLi instrument during shots 81628 and 81632. This interaction resulted in stronger Mo and Fe impurity radiations from the Mo guide plate and the collector during the two shots compared to that during the reference shot without FLiLi. After the FLiLi operation, an obvious collector melting and guide plate bottom edge damage could be observed, as shown in Fig. 15(d). Figure 16 compares the limiter design status and the actual physical status when FLiLi was inserted into the EAST vacuum vessel. The inclined angle changed from the design value of 13.5° to about 7° , due to the deformation of the FLiLi support plate, which was possible due to the thin support plate and the destructive electromagnetic force during plasma disruptions. Because the actual inclined angle was shallower than the designed angle, the bottom collector was directly exposed to the plasma. Thus, the high energy plasma melted the corner of the collector and slightly damaged the guide plate bottom edge. Furthermore, it was also noted that the TZM surface was not fully wetted by liquid Li, with a wetting percentage of about 80%. The primary reason for this lack of coverage was due to the failure of one of the EM pumps, the result of which can be clearly observed in Fig. 15(d). No Li trace is found in the blue triangular zone.

To reduce the strong plasma–material interaction at the collector corner, a slight adjustment of the FLiLi in the toroidal direction was performed. As shown in Fig. 17(a), the brighter interaction zone moved upwards to the TZM plate during shot 81633. After this adjustment, slightly reduced impurity radiation from Mo and Fe impurities was achieved. After ~ 20 shots using FLiLi, the impurity radiation decreased significantly. As shown in Fig. 17(b), it was observed that most of the limiter surface area, except for the upper right corner, was bright, likely due to a strong interaction between the flowing liquid Li and the plasma. Therefore, we speculate that this bright FLiLi area was covered by liquid Li, which is consistent with the photo captured after exposing FLiLi to air, as shown in Fig. 15(d). Finally, the decreased impurity radiation resulted from a gradually increased Li wetting area

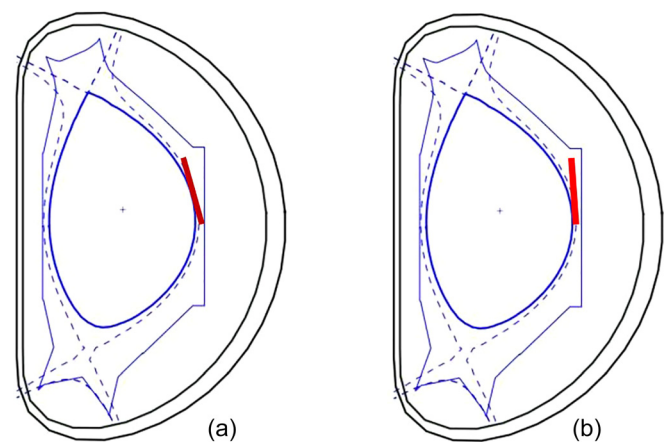


FIG. 16. Comparison of FLiLi position as designed and measured after the experiment. Shown are the (a) designed limiter inclined angle of 13.5° , (b) actual limiter inclined angle of about 7° , near vertical.

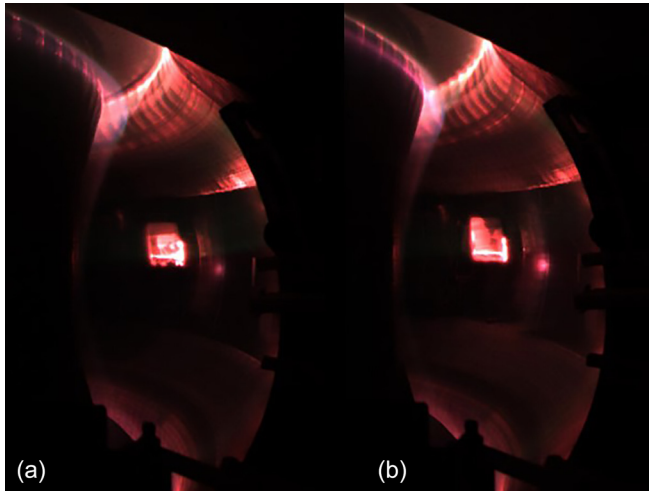


FIG. 17. Comparison of the plasma emission with a color camera during two FLiLi shots at 5 s. Shown are the (a) plasma emission in shot 81633 and (b) plasma emission in shot 81655.

on the FLiLi surface, and Li accumulation on the first wall surface due to Li evaporation, sputtering, and Li droplet ejection.

IV. DISCUSSION AND CONCLUSIONS

A TZM substrate FLiLi designed to obtain both good wettability and corrosion resistance of liquid Li has been operated in EAST. By using a TZM substrate FLiLi, fuel particle recycling continuously decreased and near-complete ELM elimination was achieved in H-mode plasmas with the RF-only heating. Compared to the first and second generation FLiLi experiments, periods of ELM mitigation were extended.

Edge recycling reduction is likely due to the enhancement of the fuel particle pumping from the Li. In addition to the pumping from the flowing liquid Li surface, the real-time renewal of the Li coating film on the first wall from the Li efflux due to Li evaporation, sputtering, and Li droplet ejection³⁵ during FLiLi operation likely contributes to the strong pumping of the fuel particles. During the third generation FLiLi operation, the Li droplet ejection caused by the destructive electromagnetic force ($\mathbf{J} \times \mathbf{B}$) was observed. The current (\mathbf{J}) resulted from both the plasma induced current and scrape-off layer currents, with magnetic field (\mathbf{B}) contributions from the toroidal and poloidal magnetic field in EAST. The liquid surface Li stability can be understood from a Rayleigh–Taylor instability analysis.²⁸ Though the design thickness of the flowing liquid Li film on the surface of FLiLi was <0.1 mm, in fact we observed a Li film thickness of 0–2 mm after exposure to air, likely because the Li flow was not uniform due to an EM pump failure. Additionally, due to the damaged collector, some liquid Li in the collector was directly exposed to the plasma, with a liquid Li depth of 1–2 cm in the collector. The critical current density into the liquid Li was not measured in our experiment, so it was assumed to be similar to NSTX,⁴² which results in a calculated stability diagram for liquid Li under the electromagnetic forces in EAST. These stability calculations show the possibility of the Li droplet ejection into the plasma during the third generation FLiLi operation.

As a result of the lower recycling source during the FLiLi operation, the edge density pedestal was reduced and shifted, the P-B mode stability boundary was expanded, and ELMs were suppressed or mitigated. These results were also successfully obtained by using Li coating or Li powder injection in NSTX⁴³ and DIII-D⁴⁴ (i.e., the peeling expansion in NSTX and the ballooning expansion in DIII-D).

The main impurities during the initial FLiLi operation were W, Mo, Fe, and Li. W and Li came from the upper W divertor and FLiLi, respectively, in the upper single-null configuration during the FLiLi operation. Mo emission had an obvious increase compared to the reference shot without FLiLi. The main reason is that, during the initial phase of the flowing liquid Li operation, liquid Li coverage was non-uniform and much of the Mo substrate was exposed to the plasma. This exposure led to impurity sputtering, which produced most of Mo impurity emission in the plasma. This process is similar to the high Fe impurity accumulation resulting from the SS substrate sputtering during the second generation FLiLi operation.¹⁷ Additionally, significant amounts of Mo and Fe impurities were generated due to the strong plasma interaction at the Mo plate edge and the SS collector resulting from the deformation of the FLiLi support plate and the change in the FLiLi angle. Over the series of FLiLi discharges, liquid Li flow on the FLiLi surface became more uniform, which resulted in a reduction of Mo impurity sputtering. Furthermore, due to Li emission from FLiLi and redeposition on the first wall surface, the continued renewal of the Li coated wall captured impurities and reduced impurity sputtering into the plasma. Therefore, impurity radiation, including both high-Z and low-Z elements, decreased significantly.

In summary, a systematic study of the application of the third generation flowing liquid Li limiter with a substrate made of TZM and its effect on recycling, impurities, and ELM behavior were presented in detail. By using a TZM substrate FLiLi, fuel particle recycling continuously decreased and a near-complete ELM elimination was achieved in H-mode plasmas with the RF-only heating. Impurity radiation, including high-Z and low-Z impurities, decreased significantly during the sequence of FLiLi operation. The decreased impurity radiation and recycling led to an increase in 10 kJ in the plasma stored energy. Engineering analysis showed a uniform lithium flow with an 80% Li cover rate similar to the second generation FLiLi achieved, even with the failure of one EM pump.

Several engineering issues still need to be resolved for the next set of experiments. The limiter support needs modification to achieve and maintain the designed limiter inclined angle. Also, a robust EM pump design is needed to achieve a 100% Li coverage on the TZM limiter guide plate surface. Furthermore, a test of a LIMIT-style FLiLi plate,⁴⁵ i.e., using a thermoelectric MHD force to drive the liquid Li flow along the surface channels, is planned for testing in both HIDRA and EAST. These efforts are aimed at generating improved designs and evaluating the feasibility of liquid Li plasma facing component for a DEMO divertor.

ACKNOWLEDGMENTS

This research is funded by the National Key Research and Development Program of China (Nos. 2017YFE0301100, 2017YFA0402500, and 2018YFE0311100), the National Natural Science Foundation of China (Nos. 11775261, 11625524, 11605246, 11075185, 11021565, 11775269, and 11905146), and in part by the U.S. Department of Energy under Contract No. DE-AC02-09CH11466.

REFERENCES

- ¹G. Federici, C. H. Skinner, J. N. Brooks, J. P. Coad, C. Grisolia, A. A. Haasz, A. Hassanein, V. Philipps, C. S. Pitcher, J. Roth *et al.*, *Nucl. Fusion* **41**, 1967 (2001).
- ²L. E. Zakharov, W. Blanchard, R. Kaita, H. Kugel, R. Majeski, and J. Timberlake, *J. Nucl. Mater.* **363–365**, 453 (2007).
- ³M. Ono, R. Majeski, M. A. Jaworski, Y. Hirooka, R. Kaita, T. K. Gray, R. Maingi, C. H. Skinner, M. Christenson, and D. N. Ruzic, *Nucl. Fusion* **57**, 116056 (2017).
- ⁴F. L. Tabares, Y. Hirooka, R. Maingi, G. Mazzitelli, V. Mirnov, R. Nygren, M. Ono, and D. N. Ruzic, *Nucl. Fusion* **56**, 127002 (2016).
- ⁵G. Mazzitelli, Y. Hirooka, J. S. Hu, S. V. Mirnov, R. Nygren, M. Shimada, M. Ono, and F. L. Tabares, *Nucl. Fusion* **55**, 027001 (2015).
- ⁶M. Ono, M. G. Bell, Y. Hirooka, R. Kaita, H. W. Kugel, G. Mazzitelli, J. E. Menard, S. V. Mirnov, M. Shimada, C. H. Skinner *et al.*, *Nucl. Fusion* **52**, 037001 (2012).
- ⁷M. Ono, M. A. Jaworski, R. Kaita, H. W. Kugel, J. W. Ahn, J. P. Allain, M. G. Bell, R. E. Bell, D. J. Clayton, J. M. Canik *et al.*, *Nucl. Fusion* **53**, 113030 (2013).
- ⁸X. Cao, D. H. Zhang, Y. J. Zhao, K. G. Xiao, J. J. Wei, S. L. Chen, X. C. Ma, and F. Gou, *Nucl. Fusion* **59**, 056015 (2019).
- ⁹S. V. Mirnov, E. A. Azizov, V. A. Evtikhin, V. B. Lazarev, I. E. Lyublinski, A. V. Vertkov, and D. Y. Prokhorov, *Plasma Phys. Controlled Fusion* **48**, 821 (2006).
- ¹⁰H. W. Kugel, M. G. Bell, R. Bell, C. Bush, D. Gates, T. Gray, R. Kaita, B. Leblanc, R. Maingi, R. Majeski *et al.*, *J. Nucl. Mater.* **363–365**, 791 (2007).
- ¹¹H. W. Kugel, D. Mansfield, R. Maingi, M. G. Bell, R. E. Bell, J. P. Allain, D. Gates, S. Gerhardt, R. Kaita, J. Kallman *et al.*, *J. Nucl. Mater.* **390–391**, 1000 (2009).
- ¹²G. Z. Zuo, J. S. Hu, S. Zhen, J. G. Li, D. K. Mansfield, B. Cao, J. H. Wu, and L. E. Zakharov, *Plasma Phys. Controlled Fusion* **54**, 015014 (2012).
- ¹³F. L. Tabarés, M. A. Ochando, F. Medina, D. Tafalla, J. A. Ferreira, E. Ascasibar, R. Balbín, T. Estrada, C. Fuentes, I. García-Cortés *et al.*, *Plasma Phys. Controlled Fusion* **50**, 124051 (2008).
- ¹⁴R. Maingi, J. S. Hu, Z. Sun, K. Tritz, G. Z. Zuo, W. Xu, M. Huang, X. C. Meng, J. M. Canik, A. Diallo *et al.*, *Nucl. Fusion* **58**, 024003 (2018).
- ¹⁵R. Lunsford, Z. Sun, R. Maingi, J. S. Hu, D. Mansfield, W. Xu, G. Z. Zuo, A. Diallo, T. Osborne, K. Tritz *et al.*, *Nucl. Fusion* **58**, 036007 (2018).
- ¹⁶P. T. Lang, R. Maingi, D. K. Mansfield, R. M. McDermott, R. Neu, E. Wolfrum, R. Arredondo Parra, M. Bernert, G. Birkenmeier, A. Diallo *et al.*, *Nucl. Fusion* **57**, 016030 (2017).
- ¹⁷G. Z. Zuo, J. S. Hu, R. Maingi, Z. Sun, Q. X. Yang, M. Huang, X. C. Meng, W. Xu, Y. Z. Qian, C. L. Li *et al.*, *Nucl. Fusion* **59**, 016009 (2019).
- ¹⁸M. Ono, M. A. Jaworski, R. Kaita, Y. Hirooka, T. K. Gray, and NSTX-U Research Team, *Fusion Eng. Des.* **117**, 124 (2017).
- ¹⁹J. Ren, G. Z. Zuo, J. S. Hu, Z. Sun, J. G. Li, L. E. Zakharov, D. N. Ruzic, and W. Y. Xu, *Fusion Eng. Des.* **102**, 36 (2016).
- ²⁰G. Z. Zuo, J. S. Hu, R. Maingi, Q. X. Yang, Z. Sun, M. Huang, Y. Chen, X. L. Yuan, X. C. Meng, W. Xu, *et al.*, *Rev. Sci. Instrum.* **88**, 123506 (2017).
- ²¹R. Majeski, S. Jardin, R. Kaita, T. Gray, P. Marfuta, J. Spaleta, J. Timberlake, L. Zakharov, G. Antar, R. Doerner *et al.*, *Nucl. Fusion* **45**, 519 (2005).
- ²²S. V. Mirnov, V. B. Lazarev, S. M. Sotnikov, V. A. Evtikhin, I. E. Lyublinski, A. V. Vertkov, and T-11M Team, *Fusion Eng. Des.* **65**, 455 (2003).
- ²³L. Chen, G. S. Xu, A. H. Nielsen, W. Gao, Y. M. Duan, H. Q. Liu, L. Wang, M. H. Li, M. Wang, X. J. Zhang *et al.*, *Nucl. Fusion* **56**, 056013 (2016).
- ²⁴G. S. Xu, B. N. Wan, J. G. Li, X. Z. Gong, J. S. Hu, J. F. Shan, H. Li, D. K. Mansfield, D. A. Humphreys, and V. Naulin, *Nucl. Fusion* **51**, 072001 (2011).
- ²⁵V. Pericoli-Ridolfini, A. Alekseyev, B. Angelini, S. V. Annibaldi, M. L. Apicella, G. Apruzzese, E. Barbato, J. Berrino, A. Bertocchi, W. Bin *et al.*, *Nucl. Fusion* **47**, S608 (2007).
- ²⁶V. Pericoli-Ridolfini, M. L. Apicella, G. Mazzitelli, O. Tudisco, R. Zagórski, and F. T. U. Team, *Plasma Phys. Controlled Fusion* **49**, S123 (2007).
- ²⁷G. Mazzitelli, M. L. Apicella, V. P. Ridolfini, G. Apruzzese, R. De Angelis, D. Frigione, E. Giovannozzi, L. Gabellieri, G. Granucci, and C. Mazzotta, *Fusion Eng. Des.* **85**, 896 (2010).
- ²⁸M. A. Jaworski, A. Khodak, and R. Kaita, *Plasma Phys. Controlled Fusion* **55**, 124040 (2013).
- ²⁹J. S. Hu, J. Ren, Z. Sun, G. Z. Zuo, Q. X. Yang, J. G. Li, D. K. Mansfield, L. E. Zakharov, D. N. Ruzic, and EAST Team, *Fusion Eng. Des.* **89**, 2875 (2014).
- ³⁰G. Z. Zuo, J. S. Hu, J. G. Li, N. C. Luo, L. E. Zakharov, L. Zhang, and A. Ti, *J. Nucl. Mater.* **415**, S1062 (2011).
- ³¹J. Ren, J. S. Hu, G. Z. Zuo, Z. Sun, J. G. Li, D. N. Ruzic, and L. E. Zakharov, *Phys. Scr.* **T159**, 014033 (2014).
- ³²G. Z. Zuo, J. Ren, J. S. Hu, Z. Sun, Q. X. Yang, J. G. Li, L. E. Zakharov, D. N. Ruzic, and HT-7 Team, *Fusion Eng. Des.* **89**, 2845 (2014).
- ³³J. Ren, G. Z. Zuo, J. S. Hu, Z. Sun, Q. X. Yang, J. G. Li, L. E. Zakharov, H. Xie, and Z. X. Chen, *Rev. Sci. Instrum.* **86**, 023504 (2015).
- ³⁴Y. Chen, Z. Wu, W. Gao, A. Ti, L. Zhang, Y. Jie, J. Zhang, J. Huang, Z. Xu, and J. Zhao, *Rev. Sci. Instrum.* **86**, 023509 (2015).
- ³⁵G. Z. Zuo, J. S. Hu, R. Maingi, J. Ren, Z. Sun, Q. X. Yang, Z. X. Chen, H. Xu, K. Tritz, L. E. Zakharov *et al.*, *Nucl. Fusion* **57**, 046017 (2017).
- ³⁶L. Zhang, S. Morita, Z. Xu, Z. Wu, P. Zhang, C. Wu, W. Gao, T. Ohishi, M. Goto, J. Shen *et al.*, *Rev. Sci. Instrum.* **86**, 123509 (2015).
- ³⁷Y. M. Wang, X. Gao, B. L. Ling, S. B. Zhang, T. Zhang, X. Han, S. C. Liu, Z. X. Liu, Y. Liu, A. Ti *et al.*, *Fusion Eng. Des.* **88**, 2950 (2013).
- ³⁸Z. Y. Zou, H. Q. Liu, Y. X. Jie, W. X. Ding, D. L. Brower, Z. X. Wang, J. S. Shen, Z. H. An, Y. Yang, L. Zeng *et al.*, *Rev. Sci. Instrum.* **85**, 11D409 (2014).
- ³⁹J. S. Hu, G. Z. Zuo, J. Ren, Q. X. Yang, Z. X. Chen, H. Xu, L. E. Zakharov, R. Maingi, C. Gentile, X. C. Meng *et al.*, *Nucl. Fusion* **56**, 046011 (2016).
- ⁴⁰L. Zhang, S. Morita, Z. Wu, Z. Xu, X. Yang, Y. Cheng, Q. Zang, H. Liu, Y. Liu, H. Zhang *et al.*, *Nucl. Instrum. Methods Phys. Res., Sect. A* **916**, 169 (2019).
- ⁴¹L. Zhang, S. Morita, Z. Xu, P. F. Zhang, Q. Zang, Y. M. Duan, H. Q. Liu, H. L. Zhao, F. Ding, T. Ohishi *et al.*, *Nucl. Mater. Energy* **12**, 774 (2017).
- ⁴²M. A. Jaworski, T. Abrams, J. P. Allain, M. G. Bell, R. E. Bell, A. Diallo, T. K. Gray, S. P. Gerhardt, R. Kaita, H. W. Kugel *et al.*, *Nucl. Fusion* **53**, 083032 (2013).
- ⁴³R. Maingi, S. M. Kaye, C. H. Skinner, D. P. Boyle, J. M. Canik, M. G. Bell, R. E. Bell, T. K. Gray, M. A. Jaworski, R. Kaita *et al.*, *Phys. Rev. Lett.* **107**, 145004 (2011).
- ⁴⁴T. H. Osborne, G. L. Jackson, Z. Yan, R. Maingi, D. K. Mansfield, B. A. Grierson, C. P. Chrobak, A. G. McLean, S. L. Allen, D. J. Battaglia *et al.*, *Nucl. Fusion* **55**, 063018 (2015).
- ⁴⁵D. N. Ruzic, W. Xu, D. Andruczyk, and M. A. Jaworski, *Nucl. Fusion* **51**, 102002 (2011).